ORIGINAL ARTICLE

IRX3 and IRX5 Inhibit Adipogenic Differentiation of Hypertrophic Chondrocytes and Promote Osteogenesis

Zhijia Tan,[1†] Mingpeng Kong,[1†] Songjia Wen,[1†] Kwok Yeung Tsang,[1] Ben Niu,[1] Christine Hartmann,[2] Danny Chan,[1] Chi-chung Hui,[3] and Kathryn S.E. Cheah[1]

[1]School of Biomedical Sciences, Li Ka Shing Faculty of Medicine, The University of Hong Kong, Pok Fu Lam, Hong Kong, HKSAR, China
[2]Institute of Musculoskeletal Medicine, Department of Bone and Skeletal Research, Faculty of Medicine, University of Münster, Münster, Germany
[3]Program in Developmental & Stem Cell Biology, The Hospital for Sick Children and Department of Molecular Genetics, University of Toronto, Toronto, ON, Canada

ABSTRACT

Maintaining the correct proportions of different cell types in the bone marrow is critical for bone function. Hypertrophic chondrocytes (HCs) and osteoblasts are a lineage continuum with a minor contribution to adipocytes, but the regulatory network is unclear. Mutations in transcription factors, IRX3 and IRX5, result in skeletal patterning defects in humans and mice. We found coexpression of *Irx3* and *Irx5* in late-stage HCs and osteoblasts in cortical and trabecular bone. *Irx3* and *Irx5* null mutants display severe bone deficiency in newborn and adult stages. Quantitative analyses of bone with different combinations of functional alleles of *Irx3* and *Irx5* suggest these two factors function in a dosage-dependent manner. In *Irx3* and *Irx5* nulls, the amount of bone marrow adipocytes was increased. In *Irx5* nulls, lineage tracing revealed that removal of *Irx3* specifically in HCs exacerbated reduction of HC-derived osteoblasts and increased the frequency of HC-derived marrow adipocytes. β-catenin loss of function and gain of function specifically in HCs affects the expression of *Irx3* and *Irx5*, suggesting IRX3 and IRX5 function downstream of WNT signaling. Our study shows that IRX3 and IRX5 regulate fate decisions in the transition of HCs to osteoblasts and to marrow adipocytes, implicating their potential roles in human skeletal homeostasis and disorders. © 2020 American Society for Bone and Mineral Research.

KEY WORDS: GENETIC ANIMAL MODELS; CELL/TISSUE SIGNALING; TRANSCRIPTION FACTORS; OSTEOBLASTS; CELLS OF BONE, GROWTH PLATE; CHONDROCYTE AND CARTILAGE BIOLOGY, MOLECULAR PATHWAYS; DEVELOPMENT; BONE MODELING AND REMODELING

Introduction

The skeleton provides protection and support for the body, but also functions as an endocrine organ that regulates metabolic homeostasis, hematopoiesis, and acute stress response.[(1–3)] Bone forms via intramembranous or endochondral ossification.[(4)] For the endochondral bones, the osteochondroprogenitors, shortly after mesenchymal condensation, differentiate into chondrocytes to form cartilage and into osteoblast progenitors in the surrounding perichondrium. The chondrocytes undergo proliferation before maturation marked by cell-cycle exit and hypertrophy to form a cartilaginous growth plate, which mediates longitudinal bone growth involving multiple lineage decisions controlled by transcription factors and signaling molecules.[(5,6)]

Recent lineage tracing studies have revealed the plasticity and extended differentiation potential of chondrocytes.[(7–9)] Hypertrophic chondrocytes (HCs) at the chondro-osseous

junction (late HCs) can switch cell fate and contribute to the full osteogenic lineage in fetal and postnatal endochondral bones. Some fetal-derived HC descendants persist into adulthood and the process is recapitulated in bone fracture healing.[(8,10–12)] Morphological and molecular analyses have suggested that the transformation of HCs to osteoblasts involves a transition to a mesenchymal-like state and cell-cycle re-entry.[(1,13)] This plasticity of chondrocytes in vivo in the growth plate is consistent with the ability of isolated skeletal stem cells to differentiate to become chondrocytes, osteoblasts, and adipocytes under specific conditions in vitro.[(9,14)] The plasticity of HCs is also illustrated by their survival and reversion to a prehypertrophic-like state when subjected to ER stress.[(15)] However, knowledge of the factors that control the fate decisions and transition from HCs to osteoblasts and other cell types are incomplete.[(16,17)]

The differentiation of chondrocytes and osteoblasts is precisely controlled by transcriptional regulators including SOX9,

RUNX2, and β-Catenin in the Wnt signaling pathway.[18–20] Canonical Wnt signaling prevents osteoblasts from differentiating into chondrocytes.[19,21] Conditional ablation of *Ctnnb1* in early osteoblast progenitors results in failure of osteoblast differentiation and switch to a chondrocytic fate. By contrast, stabilization of β-catenin in osteoblast precursors causes premature but impaired differentiation of osteoblasts.[19,21,22] HC-specific loss of β-catenin resulted in a significant reduction of trabecular bone,[23,24] but the downstream mechanisms are not clear.[17]

The Iroquois homeobox-containing transcription factors, IRX3 and IRX5, were identified as potential regulators in the HC gene regulatory network by recent study.[25] In humans, mutations in *IRX5* cause Hamamy syndrome (OMIM: 611174), a recessive congenital disorder presenting with severe skeletal defects.[26–28] *Irx3* and *Irx5* double-null mutants die from cardiac defects and skeletal malformations at mid-gestation.[29,30] Notably, osteopenia was observed in 3-week-old to 4-week-old mice with osteoblast-specific removal of *Irx3/5*.[31] IRX3 and IRX5 are also implicated in regulating the balance between beige adipose tissue (BAT) and white adipose tissue (WAT). *Irx3* null mice and transgenic mice expressing dominant-negative forms of IRX3 in adipocytes displayed resistance to weight gain and greater energy expenditure.[32,33] *Irx5* null mice also displayed reduced total fat mass and protection from obesity.[34] *IRX3* has been found to be a long-range target of human obesity-associated variants within the intron of the fat mass and obesity-associated gene *FTO*.[32,33,35,36] Therefore, IRX3 and IRX5 might function cooperatively to control fate decision of HC lineage toward osteoblasts and adipocytes during bone development.

Here we investigate the role of IRX3/5 in regulating chondrocyte to osteoblast lineage transition. IRX3 or IRX5 loss-of-function results in osteopenia. IRX3 and IRX5 control the development of trabecular and cortical bone in a dosage-dependent manner. We found that IRX3 and IRX5 are critical in HC to osteoblast lineage decision by inhibiting the adipogenic fate. HC derived osteoblasts are reduced in *Irx5* null mice, which are exacerbated by ablating *Irx3* specifically in HCs. Removal of *Irx3* and *Irx5* results in a marked switch to adipogenic fate and increased numbers of marrow adipocytes. This function of IRX3 and IRX5 is executed as downstream members of the WNT signaling pathway.

Materials and Methods

Mouse maintenance and breeding

The *Ctnnb1* floxed (loss of function) and *Ctnnb1* exon 3 floxed (gain of function)[37] (gifts of Y. Yang, Harvard University), *Irx3^LacZ/LacZ* (*Irx3^−/−*),[38] *Irx3^flox*Irx5^EGFP*/Irx3^flox*Irx5^EGFP* (*Irx5^−/−*) mice,[30] and Rosa26 tdTomato mice (*R26^td/+*)[39] have been described. Animal care and experiments were in accordance with the protocols approved by the Committee on the Use of Live Animals in Teaching and Research of the University of Hong Kong.

Immunofluorescence, immunohistochemistry, and in situ hybridization

Immunofluorescence, immunohistochemistry, and in situ hybridization were performed as described.[40,41] The antibodies used were listed: rabbit anti-GFP (1:500; Abcam, Cambridge, UK), chicken anti-β-galactosidase (1:500; Abcam), rabbit anti-RFP (1:800; Abcam), goat anti-RFP (1:500; SICGEN, Carcavelos, Portugal), rabbit anti-FABP4 (1:500; Antibody and Immunoassay

Services, University of Hong Kong, Pok Fu Lam, Hong Kong), and rabbit anti-Perilipin (1:500; Cell Signaling Technology, Beverly, MA, USA), and rabbit anti-cleaved Caspase 3 (1:200; Cell Signaling).

Micro-CT analyses of mouse skeleton

Micro-CT (μCT) imaging was performed on dissected bones using the CT scanner (Skyscan 1076; Bruker, Kontich, Belgium) at a resolution of 9 μm. The analyses on the trabecular region and cortical bone in the middle diaphysis were performed as described.[42]

Osmium tetroxide staining

Osmium tetroxide staining with μCT analyses to visualize and quantify bone marrow adipose was as described.[43] In brief, bones were fully decalcified and stained with 1% osmium tetroxide; Sigma-Aldrich, St. Louis, MO, USA for 48 to 72 hours at room temperature. After washing with Sorensen's phosphate buffer (pH = 7.4), the stained bone was embedded in 1% low-melting agarose gel and scanned again with the μCT.

X-gal staining

The skeletons of the *Irx3^LacZ* mice were dissected, all skin and muscle removed, and then fixed with 4% paraformaldehyde (PFA); Sigma-Aldrich, St. Louis, MO, USA at 4°C for 30 min. The tissues were washed (30 min × 3 times) with Rinse buffer (0.04% NP40; BDH chemicals, Poole, UK, 2mM MgCl₂, 0.02% deoxycholate, 5mM EGTA, 0.1M LiCl in PBS; ThermoFischer Scientific, Waltham, MA, USA) and stained using X-gal staining buffer (5mM K₄Fe(CN)₆; Sigma-Aldrich, St. Louis, MO, USA, 5mM K₃Fe(CN)₆; Sigma-Aldrich, St. Louis, MO, USA, 1 mg/mL X-gal; USB, Cleveland, OH, USA, 0.05 mg/mL yeast tRNA; Sigma-Aldrich, St. Louis, MO, USA in rinse buffer) in 37°C dark room for 6 hours with shaking. The paraffin section was counterstained with eosin. The X-gal signal was blue under bright field and pink under dark field.

Alcian blue staining

The paraffin sections were dewaxed and rehydrated before staining in 1% Alcian blue solution (pH 2.5); Sigma-Aldrich, St. Louis, MO, USA for 20 min then counterstained with 0.1% Nuclear Fast Red solution; Sigma-Aldrich, St. Louis, MO, USA for 5 min. The excess stains were removed by distilled water, and the slides were dehydrated and mounted with DePex; BDH Chemicals, Poole, UK.

Tartrate-resistant acid phosphatase staining

Rehydrated sections (EDTA decalcified) were incubated in 50 mL basic medium with 0.5 mL Naphthol AS-BI phosphate solution; Sigma-Aldrich, St. Louis, MO, USA (2% wt/vol in dimethyl formamide; VMR, Radnor, PA, USA) at 37°C for 1 hour. Nitrite-pararosaniline solution was freshly prepared by mixing equal volume of sodium nitrite solution (4% wt/vol sodium nitrite; BDH Chemicals, Poole, UK in H₂O) and pararosaniline dye; Sigma-Aldrich, St. Louis, MO, USA (5% wt/vol paraosaniline dye in 2 N HCL). Slides were transferred into development solution (2 mL nitrite-pararosaniline solution into 50 mL basic medium) for 5 to 12 min at 37°C before counterstaining with hematoxylin. Basic stock incubation medium (pH 4.7–5.0): 100mM sodium acetate; BDH chemicals, Poole, UK, 50mM sodium tartrate; BDH Chemicals, Poole, UK, and 0.28% vol/vol acetic acid.

Bulk RNA sequencing

Single tdTomato[+] HC descendants were manually isolated from postnatal day 5 (P5) tibial primary spongiosa under a fluorescent microscope after digestion with TrypLE Express (30 min at 37°C) (Thermo Fisher Scientific, Waltham, MA, USA). Isolated cells were pooled for each respective genotype and transferred to a hypotonic lysis solution containing RNase inhibitor, followed by cDNA synthesis according to the Smart-seq2 protocol (Illumina, San Diego, CA, USA).[44] Sequencing libraries were constructed using the Nextera XT DNA sample prep kit (Illumina). Concentration and quality of the libraries were assessed with Qubit 2.0 Fluorometer (Thermo Fisher Scientific) and Agilent 2100 high-sensitivity DNA chip (Agilent Technologies, Santa Clara, CA, USA), respectively, before sequencing at 100-bp pair-end on an Illumina HiSeq 1500 (Illumina). Exogenous spike-in RNA (preformulated blend of 92 transcripts, 250 to 2000 nucleotides long; ERCC RNA Spike-In Mix; Thermo Fisher Scientific) was used as quality control for individual samples to access the RNA degradation level, and allow for conversion of fragments per kilobase million (FPKM) values to transcripts per cell. All primary sequencing data were deposited in the GEO website (GSE146111; https://www.ncbi.nlm.nih.gov/geo/).

Bioinformatic analyses of RNA sequencing data

All Smart-seq2 sequencing data were individually aligned to the reference mouse genome (mm10) and gene expression (FPKM values) was calculated for each transcript using the TopHat and Cufflinks package.[45] The high-throughput sequencing (HTS) HTSeq package sequencing read count was calculated as described.[46]

Cell culture, DNA transfection, and luciferase assay

Dual luciferase assay was performed as described.[25] In brief, ATDC5 cells were grown to ~70% to 80% confluency before transfection with pGL3-basic luciferase reporters (Promega, Madison, WI, USA) containing regulatory elements from *Irx3* (−951 bp to +225 bp) and *Irx5* (−1825 bp to +96 bp) loci and pCDNA-mWnt3a vector (gift of Dr. Bo Gao, The University of Hong Kong; Original pCDNA vector; Addgene, Watertown, MA, USA) using Lipofectamine 2000 (Invitrogen, Carlsbad, CA, USA). Luciferase activity was measured according to the manufacturer's instructions (Dual Luciferase Reporter Assay Kit; Promega, San Luis Obispo, CA, USA). Luciferase expression was calculated as a fold-change relative to the activity of *Renilla* luciferase.

Statistics

Mice analyzed at different ages were of mixed gender. Data presented are the averages with standard deviation ($n \geq 3$). Statistical significance level was evaluated by Student's t test (two-tailed, unpaired) between two groups, or one-way ANOVA, Tukey's multiple comparisons test among three groups. The difference with $p < .05$ is considered to be significant.

Results

Irx3 and *Irx5* are expressed in late hypertrophic chondrocytes and osteoblasts

Transcriptome data from different regions of the developing mouse growth plate[25] showed peak expression of *Irx3* and *Irx5* in late HCs (Fig. 1A,D). We characterized the expression patterns of *Irx3* and *Irx5* in genetic reporter mice (*Irx3*[LacZ/+] and *Irx5*[EGFP/+]).[30] In the tibial growth plate, *Irx3* was expressed in late HCs and osteoblasts in the trabecular region, periosteum, and endosteum, and in osteocytes in cortical bone (Fig. 1B,C). *Irx5* showed a similar expression pattern to *Irx3* (Fig. 1E,F). Co-staining of beta-galactosidase (LacZ) and enhanced green fluorescent protein (EGFP) in *Irx3*[LacZ]*Irx5*^{+};*Irx3*^{+}*Irx5*[EGFP] mice indicate that *Irx3* and *Irx5* are coexpressed in the osteoblast lineage (Fig. 1G–I). To investigate the role of *Irx3* and *Irx5* in bone development and lineage differentiation, we examined the skeletal morphologies of *Irx3*^{−/−} (*Irx3*[LacZ/LacZ]) and *Irx5*^{−/−} (*Irx5*[EGFP/EGFP]) single knockout mice with control mice. *Irx3*^{−/−} and *Irx5*^{−/−} mice showed reduced body weight and generalized shortening of body length (nose tip to tail base) (Fig. 1J,K; Supplemental Fig. S1). X-rays showed reduced bone mineralization intensity in *Irx3*^{−/−} and *Irx5*^{−/−} mice comparing to control littermates (Fig. 1L–O; Supplemental Fig. S1), suggesting that IRX3 and IRX5 are crucial for both bone development and homeostasis.

Removal of *Irx3* and *Irx5* results in impaired osteoblast differentiation and reduced bone formation

To understand whether the bone loss in *Irx3* and *Irx5* mutants is a developmental defect, we first examined the developing growth plate and bones at the fetal stage embryonic day 15.5 (E15.5). Here the calcification of the primary spongiosa in the bone marrow cavity was reduced in *Irx3* and *Irx5* mutants, as visualized by Alcian blue and von Kossa staining (Fig. 2A,B). Histological examination of tibias from P10 and 4-week-old littermates revealed osteoporotic phenotypes in the proximal and distal trabecular regions and thinner cortical bone in *Irx3*^{−/−} (Fig. 2C,G; Supplemental Fig. S2A,I,M) and *Irx5*^{−/−} mice (Fig. 2K,O; Supplemental Fig. S2E,Q,U). At the 4-week stage, histology and in situ hybridization of HC-specific marker *Col10a1*, showed no significant change in the size of the hypertrophic zone with removal of IRX3 or IRX5 (Supplemental Fig. S3A, a'–c'). μCT analyses revealed marked decreases in proximal and distal trabecular bone volume concerning total volume (BV/TV) and bone mineral density (BMD) in *Irx3*^{−/−} (Fig. 2D–F; Supplemental Fig. S2B-D,J–L) and *Irx5*^{−/−} (Fig. 2L–N; Supplemental Fig. S2F-H,R–T) mice compared to wild-type or heterozygous littermates. Cortical bone thickness and density were also reduced in *Irx3*^{−/−} (Fig. 2H–J; Supplemental Fig.S2N–P) and *Irx5*^{−/−} (Fig. 2P–R; Supplemental Fig. S2V–X) mice. The generalized reduction in cortical and trabecular bone in the *Irx3* and *Irx5* mutants is therefore consistent with their expression pattern.

To elucidate the mechanism(s) underlying bone loss in *Irx3* and *Irx5* null mice, we next examined the molecular markers in trabecular and cortical bones. In situ hybridization showed the number of cells expressing the osteoblastic marker *Col1a1* in the trabecular regions was decreased (Supplemental Fig. S3A, d'–f') and the intensity of *Col1a1* staining in the cortical bones was reduced (Supplemental Fig. S3A, g'–i'). The number of mature osteocytes labeled by SOST was markedly reduced in the cortical bone from *Irx3* and *Irx5* null mice (Supplemental Fig. S3B, a'–d'). Thus, removal of *Irx3* or *Irx5* impairs osteoblast differentiation from embryonic to adult stages.

Given that *Irx3* and *Irx5* are expressed in late HCs and osteoblasts, and HCs become osteoblasts in endochondral bone development, we characterized mouse mutants with different *Irx* gene dosage in HCs (denoted by the number of functional alleles for *Irx3* and *Irx5*; eg, wild-type for *Irx3*;*Irx5* is 2;2, compound
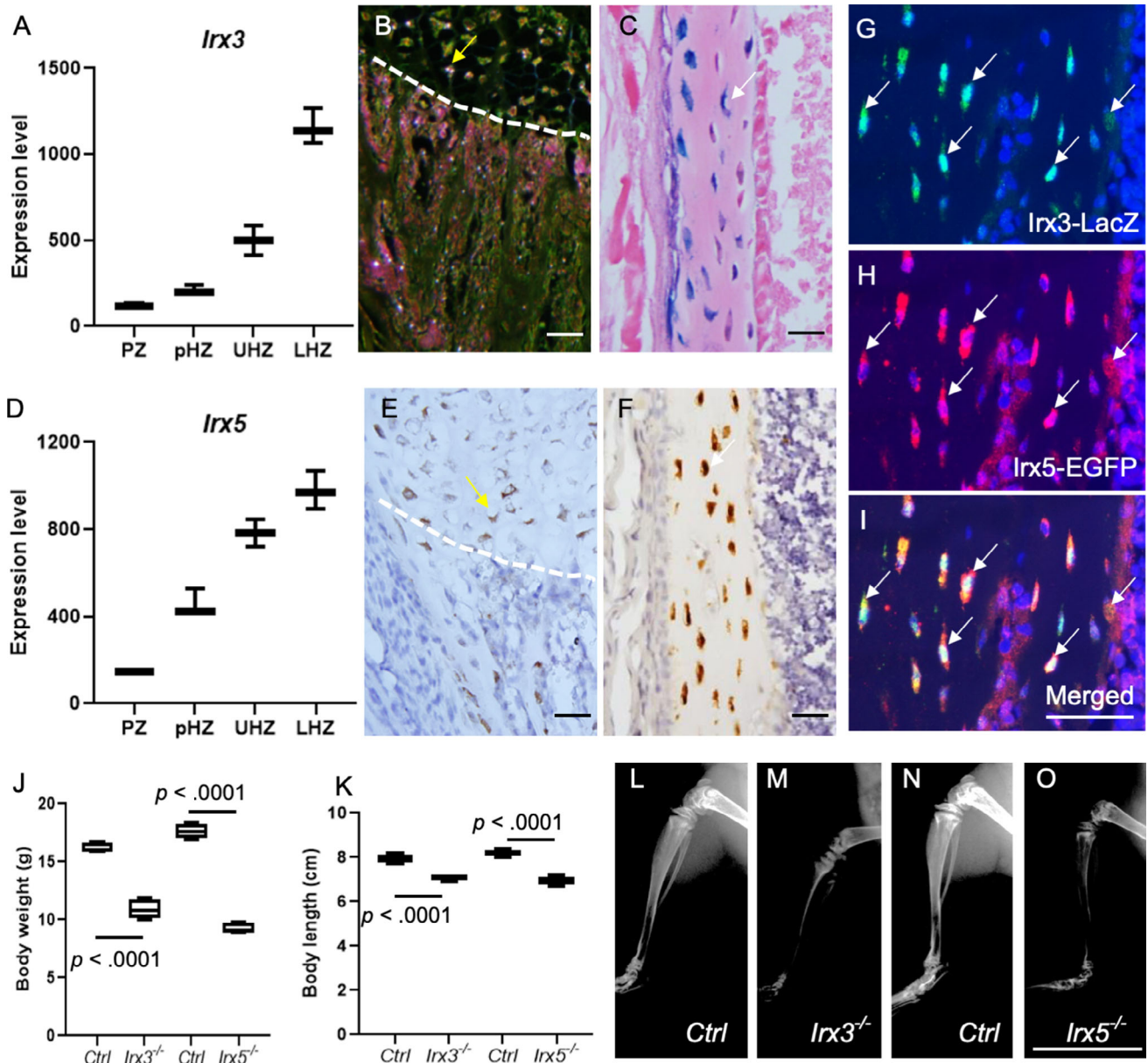
Fig 1. Expression patterns of *Irx3* and *Irx5* in chondrocytes and osteoblasts. (*A,D*) Microarray expression pattern of *Irx3* (*A*) and *Irx5* (*D*). (*B,C*) Endogenous *Irx3* expression pattern revealed by X-gal staining of *Irx3*$^{LacZ/+}$ mice at P10 stage. Dark field (*B*) is shown for the growth plate and trabecular region. Bright field (*C*) is shown for cortical bone. Scale bar = 100 μm. (*E,F*) Endogenous IRX5 expression pattern reflected by staining of EGFP on P10 *Irx5*$^{EGFP/+}$ mice in the growth plate (*E*) and cortical bone (*F*). White dotted line indicates chondro-osseous junction. The arrows point to *Irx3* or *Irx5* expressing HCs and osteocytes, respectively. (*G–I*) Coexpression of IRX3 and IRX5 shown by staining of β-galactosidase (green), EGFP (Red) and DAPI (blue), on the cortical bones from *Irx3*^{LacZ}*Irx5*$^+$/ *Irx3*$^+$*Irx5*^{EGFP} mice. Osteocytes in the cortical bone and osteoblasts in the endosteum were arrowed. (*J,K*) Comparison of body weight and body length in *Irx3*$^{-/-}$ and *Irx5*$^{-/-}$ mice with corresponding controls. (*L–O*) Bone density of tibias shown by X-ray in *Irx3*$^{-/-}$, *Irx5*$^{-/-}$ mice and littermate controls. Scale bar = 1 cm. Data presented are the averages with standard deviations from five animals per genotype. Values of *p* calculated by Student's *t* test, two-tailed, unpaired. Scale bar = 100 μm. PZ = proliferating zone; pHZ = pre-hypertrophic zone; UHZ = upper hypertrophic zone; LHZ = lower hypertrophic zone.

heterozygote *Irx3*$^+$*Irx5*$^+$/*Irx3*$^-$*Irx5*$^{/-}$, is 1;1, and so on. Functional alleles for conditional HC mutants generated by *Col10a1-Cre*[8] are denoted as *Irx3*$^{ΔHC/ΔHC}$ and 0^{ΔHC}). We focused on the trabecular region where late HCs become osteoblasts, to test whether *Irx3* and *Irx5* regulate endochondral bone formation in a dosage-dependent way. Mineralization density was progressively decreased with the loss of *Irx* gene dosage compared to wild-type and heterozygous controls (Supplemental Fig. S4).

Quantification of bone volume by μCT analyses showed that bone formation was reduced by 31.97% in *Irx3*$^-$*Irx5*$^+$/*Irx3*$^-$*Irx5*$^+$ (0;2, *Irx3*$^{-/-}$) and by 35.34% in *Irx3*$^+$*Irx5*$^-$/*Irx3*$^+$*Irx5*$^-$ (2;0, *Irx5*$^{-/-}$) (Fig. 2*S*). Complete removal of both *Irx* genes in HCs (0^{ΔHC};0, *Irx3*^{ΔHC}*Irx5*$^-$/*Irx3*^{ΔHC}*Irx5*$^-$), impacted more severely, leading to a 53.25% reduction in bone volume (Fig. 2*S*). Overall, increasing severity of skeletal defects, such as reduced trabecular bone ossification, was correlated with the removal of functional *Irx3* and
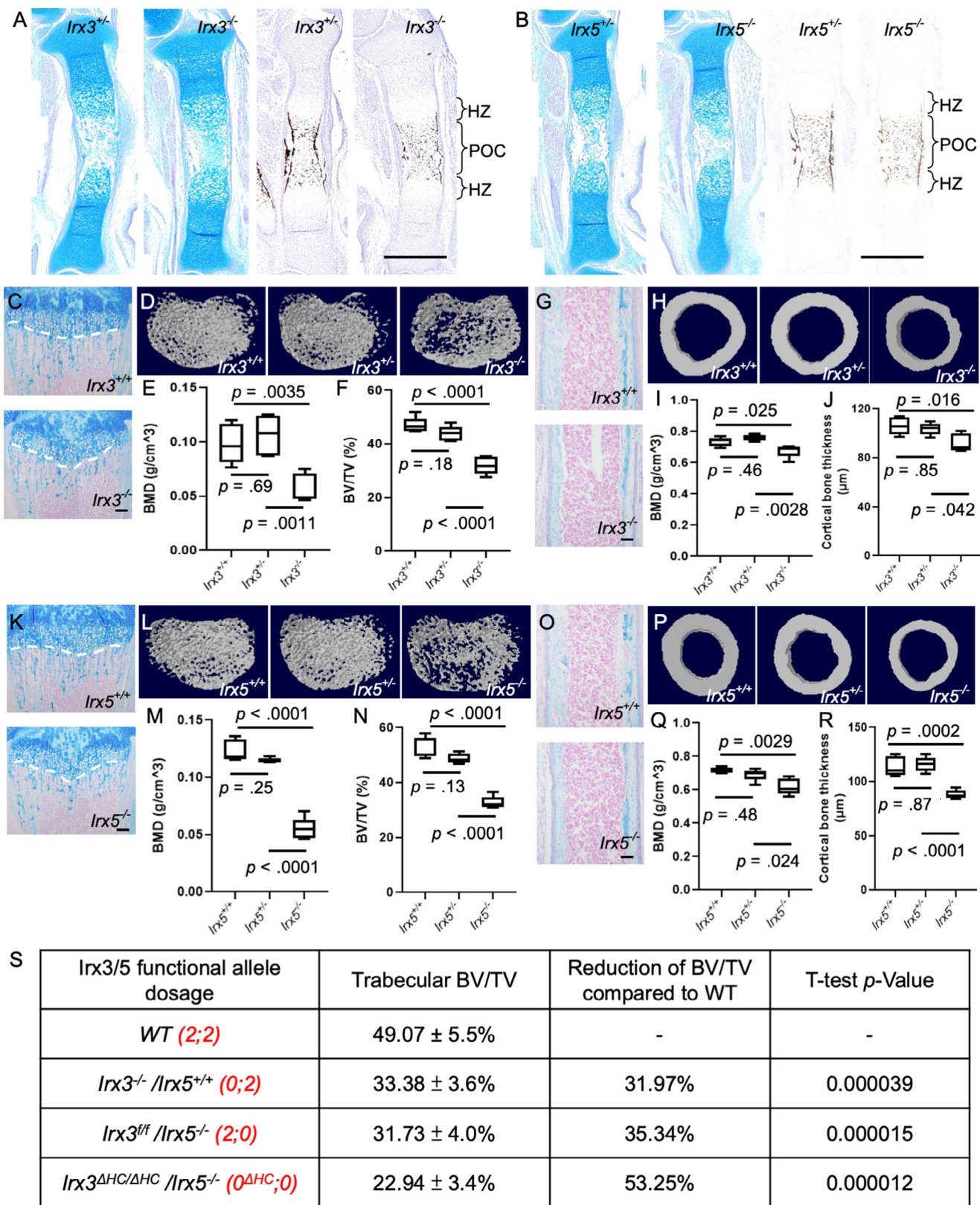
Irx3/5 functional allele dosage	Trabecular BV/TV	Reduction of BV/TV compared to WT	T-test *p*-Value
WT (2;2)	49.07 ± 5.5%	-	-
Irx3⁻/⁻ /Irx5⁺/⁺ (0;2)	33.38 ± 3.6%	31.97%	0.000039
Irx3ᶠ/ᶠ /Irx5⁻/⁻ (2;0)	31.73 ± 4.0%	35.34%	0.000015
Irx3ᐃHC/ᐃHC /Irx5⁻/⁻ (0ᐃHC;0)	22.94 ± 3.4%	53.25%	0.000012

Fig 2. Reduced bone formation in *Irx3⁻/⁻* and *Irx5⁻/⁻* mutant mice. (*A,B*) Alcian blue and von Kossa staining on tibia sections from *Irx3⁺/⁻* and *Irx3⁻/⁻* (*A*), *Irx5⁺/⁻* and *Irx5⁻/⁻* (*B*) mice at E15.5 (Embryonic Day 15.5). (*C*) Alcian blue stained proximal tibias from *Irx3⁺/⁻* and *Irx3⁻/⁻* mice at P10 stage. (*D*) Representative μCT reconstruction of proximal tibias from P10 *Irx3⁺/⁺*, *Irx3⁺/⁻* and *Irx3⁻/⁻* littermates. (*E,F*) Analyses of the trabecular BMD (one-way ANOVA *p* = .0008) and trabecular BV/TV (one-way ANOVA *p* < .0001) in *Irx3⁻/⁻* mutants as compared to *Irx3⁺/⁺* and *Irx3⁺/⁻* controls (*p* values between different groups calculated by Tukey's multiple comparisons test were shown in the box plot). (*G*) Alcian blue–stained cortical bones from *Irx3⁺/⁻* and *Irx3⁻/⁻* mice.

Irx5 alleles, confirming their dosage dependent functions during bone development.

IRX3 and IRX5 direct the HC lineage toward osteogenic cell fate

Bone homeostasis is maintained by the balance between formation by osteoblasts and resorption by osteoclasts.[47] We compared the frequency of tartrate-resistant acid phosphatase (TRAP) expressing osteoclasts in the trabecular region of mutants versus littermate controls. The numbers of TRAP$^+$ osteoclasts were comparable in *Irx3*$^{-/-}$ and *Irx5*$^{-/-}$ mice with corresponding controls (Supplemental Fig. S5A–E). Staining of cleaved caspase 3 also showed similar numbers of apoptotic cells among these littermates (Supplemental Fig. S5F–J), ruling out the possibility that reduced bone formation in mutants was caused by increased apoptosis in osteoblasts. Given that *Irx3* and *Irx5* were expressed in the lower hypertrophic zone, and HCs can become osteoblasts,[8] the loss of these two genes may affect the chondrocyte lineage progression to osteoblasts. We used the *Col10a1-Cre*: *R26*$^{td/+}$ reporter system to trace HCs in *Irx3*$^{-/-}$ mice. Fewer HC descendants were detected in the primary spongiosa of *Irx3*$^{-/-}$ and *Irx3*$^{\Delta HC}$*Irx5*$^-$/*Irx3*$^{\Delta HC}$*Irx5*$^-$ mice compared with heterozygous littermates (Fig. 3A,B,D,E). Quantitative analyses showed that the numbers of HC descendants were reduced by approximately 42% and 45%, respectively, in *Irx3*$^{-/-}$ and *Irx3*$^{\Delta HC}$*Irx5*$^-$/*Irx3*$^{\Delta HC}$*Irx5*$^-$ mice compared with controls (Fig. 3C,F). This suggested that *Irx3* and *Irx5* might play important roles in the lineage progression of HCs.

To test whether the HC-to-osteoblast transition was defective in *Irx3* and *Irx5* compound mutants, we used tdTomato staining coupled with *Col1a1* in situ hybridization to quantify the number of HC-derived osteoblasts. Within the primary spongiosa, the *Irx3*$^{\Delta HC}$*Irx5*$^-$/*Irx3*$^{\Delta HC}$*Irx5*$^-$ mice displayed fewer *Col1a1* expressing cells. Fewer double-labeled (Td$^+$/*Col1a1*$^+$) HC-derived osteoblasts were detected in the mutant trabecular region (Fig. 4A–E). In *Irx3*$^{\Delta HC}$*Irx5*$^-$/*Irx3*$^{\Delta HC}$*Irx5*$^-$ mice, the fraction of differentiated osteoblasts of HC origin (Td$^+$/*Col1a1*$^+$ cells) as a proportion of total HC descendants (Td$^+$ cells) was only 21.34%, in contrast to 34.76% in *Irx3*$^+$*Irx5*$^+$/*Irx3*$^+$*Irx5*$^+$ mice (2;2, the wild type) (Fig. 4F). The contribution of HC-derived osteoblasts to the entire osteoblast pool in the trabecular and endosteal compartments was also lower in the mutants. The percentage of HC-derived Td$^+$/*Col1a1*$^+$ cells as a proportion of total *Col1a1*$^+$ cells in *Irx3*$^{\Delta HC}$*Irx5*$^-$/*Irx3*$^{\Delta HC}$*Irx5*$^-$ mice dropped approximately 25% compared to the wild-type control (Fig. 4G). Additionally, co-staining for tdTomato and osterix shows that fewer double-labeled (Td$^+$/Osterix$^+$) osteoblasts are found in mutant compared to heterozygous control, in trabecular region of the distal tibia (Supplemental Fig. S7A–D). These data indicate that ablation of *Irx3* and *Irx5* in HCs impaired their transition and differentiation to osteoblasts, reducing the contribution of HC-derived osteoblasts to endochondral bone.

Loss of *Irx3* and *Irx5* increases the HC transition toward adipocytes

Given that human *IRX3* is associated with adipogenesis and obesity,[32,33] and HCs can become osteoblasts and adipocytes in zebrafish[48] and mice,[49] we investigated whether the decrease of HC-derived osteoblasts was caused by a lineage shift toward adipocytes. By coupling osmium tetroxide staining and μCT analysis, we found a significant increase of adipocyte tissue in the bone marrow of *Irx3*$^{-/-}$ and *Irx5*$^{-/-}$ mutants compared with heterozygotes (Fig. 5A–E). Staining using adipocyte markers Perilipin and FABP4 showed that more adipocytes were present in *Irx3* and *Irx5* single null mutants in distal tibia (Fig. 5F–J; Supplemental Fig. S6A–E), suggesting IRX3 and IRX5 negatively regulate adipogenesis in the HC-lineage descendants. Consistent with osmium tetroxide staining, no adipocytes can be detected in proximal tibias on P10 either in wild-type or *Irx3/5* mutants (Supplemental Fig. S7E,F). This finding is consistent with the reported variation in adipocyte development between proximal and distal tibias.[50]

To investigate whether specific ablation of *Irx3* and *Irx5* would affect the fate determination of HC-derived cells, we double-labeled cells with HC lineage marker and adipocyte marker Perilipin at the early initiation stage of marrow adipogenesis. A small portion of Perilipin$^+$ adipocytes colocalized with tdTomato (driven by *Col10a1*-Cre) at the distal tibia of P10 mice (Fig. 6A,C), implying that in wild-type mice, HC descendants are able to differentiate to adipocytes in the primary spongiosa. Interestingly, *Irx3*$^{\Delta HC}$*Irx5*$^-$/*Irx3*$^{\Delta HC}$*Irx5*$^-$ mice displayed more double-positive HC-derived adipocytes (Td$^+$/Perilipin$^+$) than the heterozygous control (Fig. 6A–D). The Td$^+$ descendants was approximately 30% lower in the *Irx* mutants (Fig. 6E), whereas the Perilipin$^+$ adipocytes was about 50% higher than controls (Fig. 6F). The HC-derived Td$^+$/Perilipin$^+$ adipocytes was about doubled in the mutants compared to controls (Fig. 6G). The percentage of double-labeled cells among the HC descendants (Td$^+$) increased from 1.4% in controls to 4.8% in mutants (Fig. 6H), indicating that more HC descendants became adipocytes instead of osteoblasts. Among Perilipin$^+$ adipocytes, 31% HC-derived cells were found in control mice, compared with 48% in the mutants (Fig. 6I). However, the total numbers of non-Td$^+$ adipocytes

---

(H) Representative μCT reconstruction of cortical bones from *Irx3*$^{+/+}$, *Irx3*$^{+/-}$, and *Irx3*$^{-/-}$ littermates. (I,J) Analyses of the cortical bone density (one-way ANOVA p = .0031) and thickness (one-way ANOVA p = .013) in *Irx3*$^{+/+}$, *Irx3*$^{+/-}$ and *Irx3*$^{-/-}$ littermates (p values between different groups calculated by Tukey's multiple comparisons test are shown in the box plot). (K) Alcian blue–stained proximal tibias from *Irx5*$^{+/+}$ and *Irx5*$^{-/-}$ mice at P10 stage. (L) Representative μCT reconstruction of proximal tibias from *Irx5*$^{+/+}$, *Irx5*$^{+/-}$, and *Irx5*$^{-/-}$ littermates. (M,N) Analyses of the trabecular BMD (one-way ANOVA p < .0001) and BV/TV (one-way ANOVA p < .0001) in *Irx5*$^{-/-}$ mutants as compared to *Irx5*$^{+/+}$ and *Irx5*$^{+/-}$ controls (p values between different groups calculated by Tukey's multiple comparisons test were shown in the box plot). (O) Alcian blue–stained cortical bones from P10 old *Irx5*$^{+/+}$ and *Irx5*$^{-/-}$ mice. (P) Representative μCT reconstruction of cortical bones from *Irx5*$^{+/+}$, *Irx5*$^{+/-}$, and *Irx5*$^{-/-}$ littermates. (Q,R) Analyses of the cortical bone density (one-way ANOVA p = .0031) and thickness (one-way ANOVA p < .0001) from *Irx5*$^{+/+}$, *Irx5*$^{+/-}$, and *Irx5*$^{-/-}$ littermates (p values between different groups calculated by Tukey's multiple comparisons test were shown in the box plot). (S) Comparison of trabecular BV/TV between WT with different dosages of functional *Irx3/5* allele. Bracketed numbers indicate the functional gene dosages of *Irx3* and *Irx5*, respectively. Data presented are the averages with standard deviations from five animals per genotype. Values of p calculated by Student's t test, two-tailed, unpaired. Scale bar = 100 μm. BMD = bone mineral density; BV/TV = bone volume over total volume; HZ = hypertrophic zone; POC = primary ossification center.
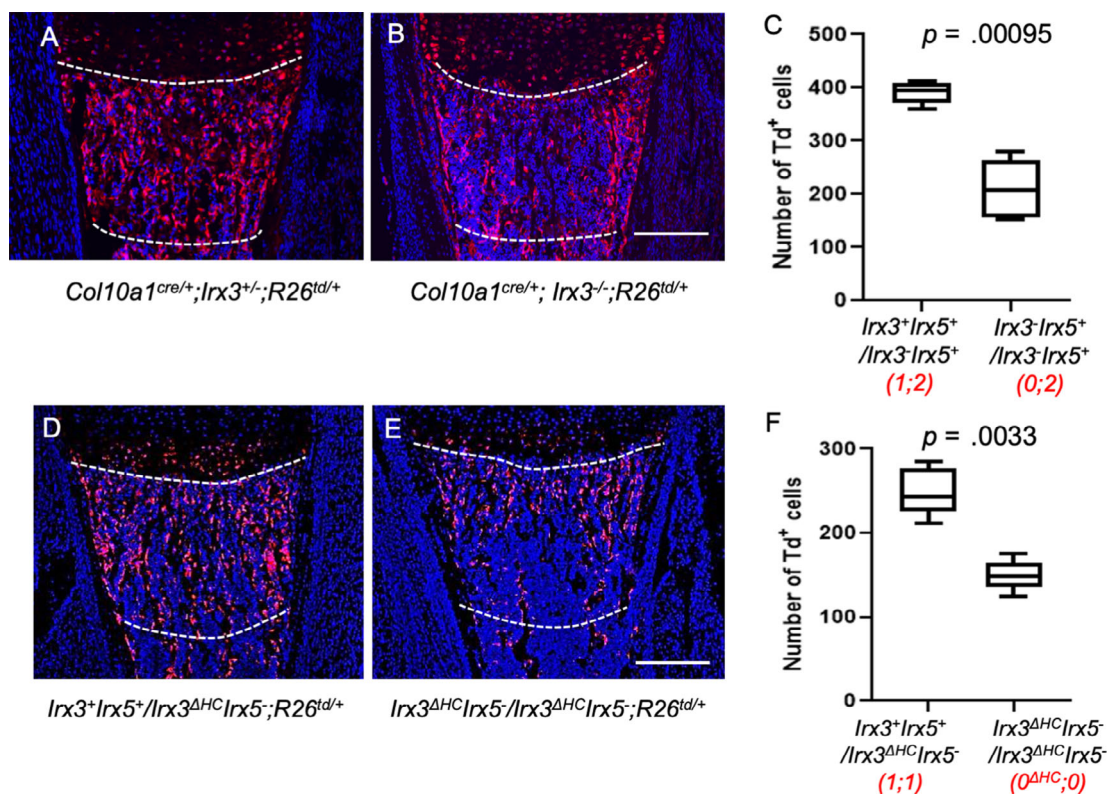
Fig 3. Reduced HC descendants in $Irx3^{-/-}$ and $Irx3^{\Delta HC}Irx5^-/Irx3^{\Delta HC}Irx5^-$ mutants. (A,B) Staining of tdTomato on proximal tibia sections from P5 $Col10a1^{cre/+}$; $Irx3^{-/-}$; $R26^{tom/+}$ mutants and littermate heterozygous controls. (C) Quantification of tdTomato-positive descendants in the trabecular region 200 μm beneath the chondro-osseous junction in A and B (dotted line region) (D,E) Staining of tdTomato on proximal tibia sections from P5 $Irx3^{\Delta HC}Irx5^-/Irx3^{\Delta HC}Irx5^-$;$R26^{td/+}$mutants and littermate heterozygous controls. (F) Quantification of tdTomato-positive descendants in the trabecular region 200 μm beneath the chondro-osseous junction in D and E (dotted line region). Data are displayed as averages with standard deviations from five nonconsecutive sections in three animals of each genotype. Values of p calculated by Student's t test, two-tailed, unpaired. Scale bar = 100 μm.

were comparable between mutants and control littermates (Fig. 6J). This observation suggested that the increased portion of adipocytes were mainly derived from HCs. Overall, removal of Irx3 and Irx5 function in HCs disrupted the lineage extension to osteoblasts and skewed the fate of HC descendants toward adipogenesis.

In addition to appendicular bone, we also found fate change of HC descendants in vertebrae. Fewer HC descendants and HC-derived osteoblasts (labeled by Td⁺/Osterix⁺) were observed in sacral vertebrae in Irx3/5 mutants (Supplemental Fig. S7G–L). Similar to tibia, more HC-derived adipocytes (Td⁺/Perilipin+) can be identified in sacral vertebrae of mutants compared to heterozygous controls (Supplemental Fig S7M,N). Therefore loss of Irx3/5 function leads to a similar change in cell fate in both the appendicular and axial skeleton.

To clarify the above changes in the cell population composition upon ablation of IRX3 and IRX5, we compared the percentages of HC-derived and non–HC-derived osteoblasts and adipocytes in the Irx3/5 mutants and corresponding controls. The total HC-derived population (Td⁺ cells) was reduced at both P5 and P10 stages (Supplemental Fig. S8A,C), though the degree of reduction was not to the same extent (45.3% at P5 and 31.4% at P10), reflecting possible differences in postnatal growth stages. The HC-derived osteoblasts (Col1a1⁺/Td⁺ cells) dramatically decreased (Supplemental Fig. S8A,B), while the HC-derived

adipocytes (Perilipin⁺/Td⁺ cells) were significantly increased (Supplemental Fig. S8C,D), regardless of whether as a proportion of total Td⁺ descendants or total Perilipin⁺ adipocytes. However, the percentage of non–HC-derived osteoblasts (Col1a1⁺/Td⁻ cells) was also decreased in the Irx3/5 mutants (Supplemental Fig. S8B). Because IRX5 is required for osteoblast differentiation in endochondral and membranous bones,[31] this result could be due to the complete absence of Irx5 in both HC derived and non–HC-derived lineages in the mutants. Interestingly, the percentages of non–HC-derived adipocytes (Perilipin⁺/Td⁻ cells) were comparable between mutants and controls (Supplemental Fig. S8D), suggesting that IRX5 does not control or is dispensable for the differentiation of non–HC-derived marrow adipocytes when IRX3 is intact.

Irx3 and Irx5 are downstream targets of Wnt/β-catenin that direct HCs toward the osteogenic lineage by inhibiting adipogenesis

Stabilization of β-catenin in late HCs is crucial for trabecular bone formation and differentiation of HC-derived osteoblasts.[23,24] Canonical Wnt signaling represses adipogenesis of white adipose tissue,[51] and removal of β-catenin in pre-osteoblasts alters the cell fate balance from osteogenesis toward adipogenesis.[52] Because Irx3 is a direct target of β-catenin during neural axis
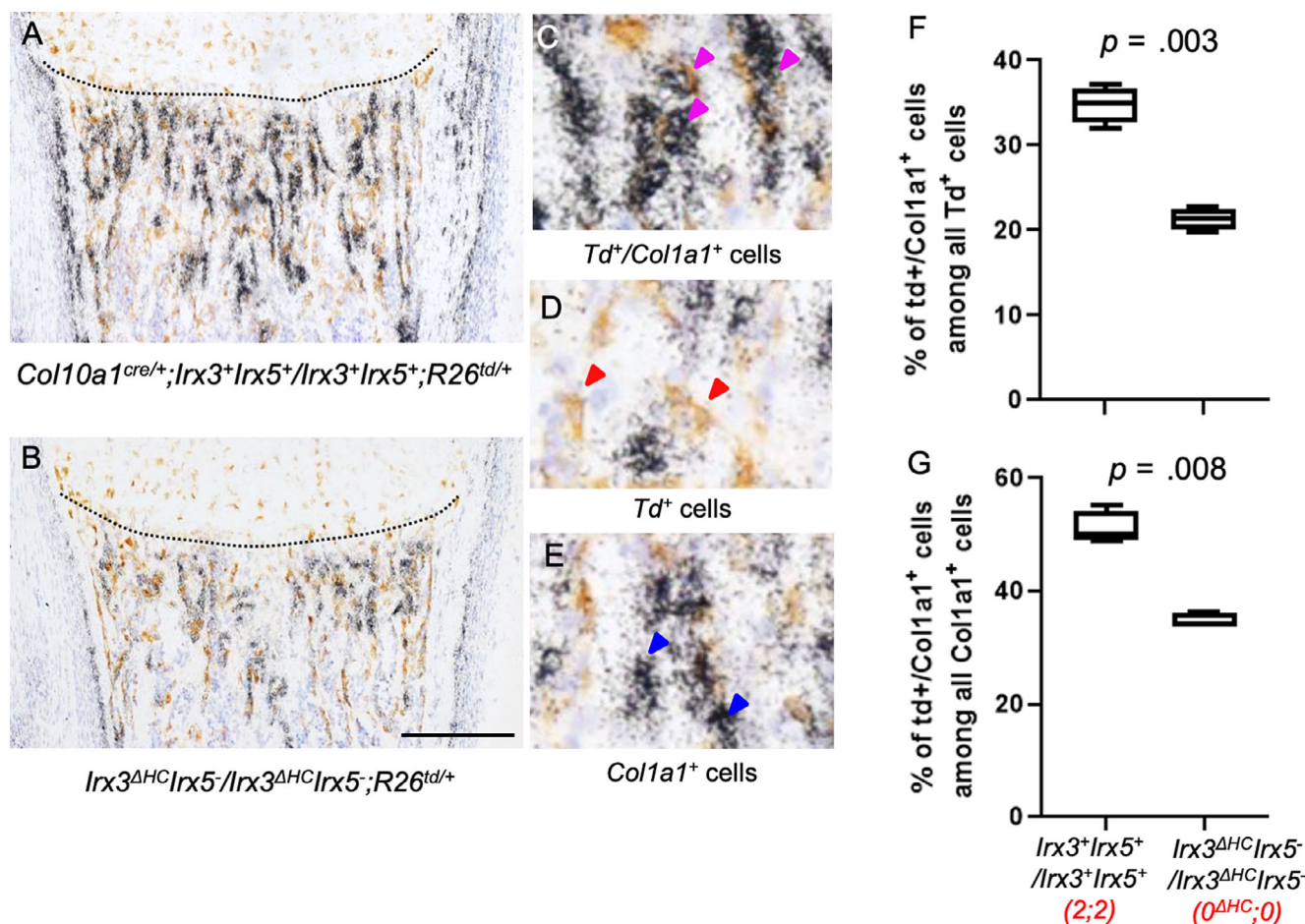
Fig 4. Reduced frequency of HC-derived osteoblasts in $Irx3^{\Delta HC}Irx5^-/Irx3^{\Delta HC}Irx5^-$ mutants. (A,B) Staining of tdTomato (brown) followed by in situ hybridization with *Col1a1* (black) on proximal tibia sections from P5 $Irx3^{\Delta HC}Irx5^-/Irx3^{\Delta HC}Irx5^-;R26^{td/+}$ mutants and littermate controls. Black dotted line indicates chondro-osseous junction. (C–E) *Col1a1*⁺/tdTomato⁺ (pink arrows), tdTomato⁺ cells (red arrows) and *Col1a1*⁺ (blue arrows) cells in the trabecular regions are shown at higher magnification. (F,G) Quantification of *Col1a1*⁺/tdTomato⁺ cells in the trabecular regions from mutant and control mice relative to HC descendants (all tdTomato⁺) and osteoblasts (all *Col1a1*⁺), respectively. Data are displayed as averages with standard deviations from five nonconsecutive sections in three animals of each genotype. Values of *p* calculated by Student's *t* test, two-tailed, unpaired. Scale bar = 100 μm.

patterning in *Xenopus*,[53] we tested whether IRX3 and IRX5 mediate Wnt signaling in HCs and descendants by determining the impact of HC-specific loss-of-function or gain-of function of β-catenin on their expression levels in vivo. For this, 70 HC-descendant cells were isolated from the proximal tibia of each pup (two controls, four β-catenin loss-of-function, and two β-catenin gain-of-function mutants at P5 stage) for bulk RNA sequencing. Expression of *Irx3* and *Irx5* was markedly decreased as a result of HC-specific β-catenin loss-of-function and by contrast were increased in the gain-of-function HC-*Ctnnb1* mutants (Fig. 7A), suggesting that *Irx3* and *Irx5* are downstream targets of β-catenin in HC descendants. To explore this regulatory prediction, we examined the in vivo derived chromatin immunoprecipitation followed by sequencing (ChIP–seq) data of β-catenin in *Xenopus*[54] and found significant presence of β-catenin-bound regions in the promoter and intergenic regions of *Irx3* and *Irx5* loci. We cloned the proximal promoter regions of *Irx3* and *Irx5* containing conserved canonical T-cell specific transcription factor/lymphoid enhancer binding factor (TCF/LEF) binding motifs[55] into a luciferase reporter vector and tested the ability

of exogenous Wnt3a to mediate transactivation of the expression of these reporters in ATDC5 cells, a chondrogenic cell line[56] (Fig. 7B,C). Increasing doses of *Wnt3a* overexpression drove corresponding increases in *Irx3* and *Irx5* promoter-driven luciferase reporter activities, consistent with their regulation by Wnt/β-catenin signaling in vivo (Fig. 7A).

Discussion

The discovery of the HC-to-osteoblast lineage continuum has added a new dimension to concepts of the lineage origin of osteoblasts in the endochondral bones and other cell types in the bone marrow.[16,17] We have shown the potential of HCs to contribute to osteoblast and adipocyte lineages. By combining analyses of the phenotypic and cellular impact of reducing the dosage of *Irx3* and *Irx5* in single and compound null mutants, with HC-specific lineage tracing, we have revealed a dosage-dependent role of IRX3 and IRX5 in the control of bone development and HC lineage transition, affecting the cellular
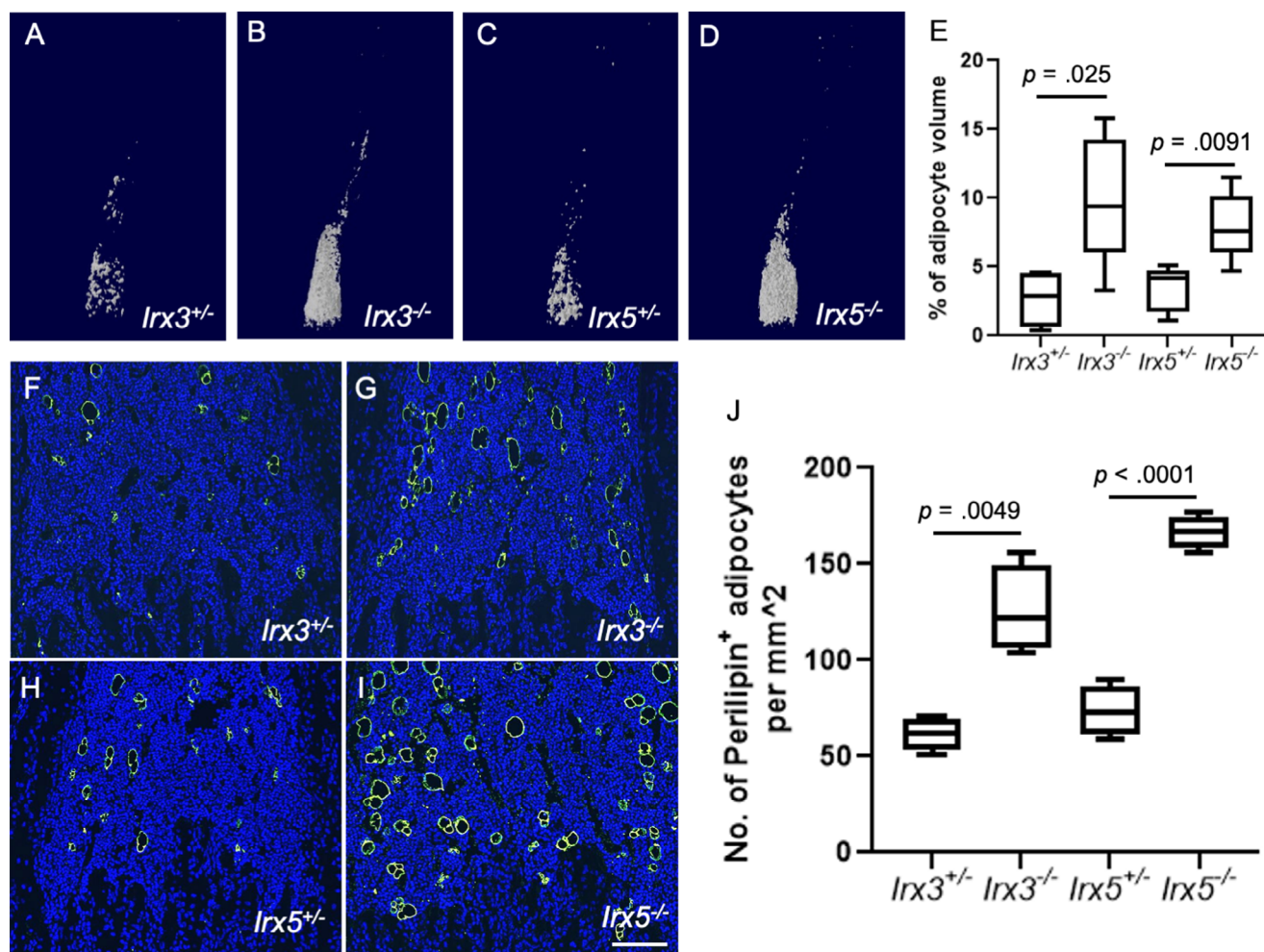
Fig 5. Depletion of *Irx3* and *Irx5* results in elevated amounts of marrow adipocytes. (*A–D*) Osmium tetroxide staining and μCT reconstruction of the tibias from P10 *Irx3*$^{-/-}$ and *Irx5*$^{-/-}$ mutants and heterozygous controls. (*E*) Quantification of percentage of bone marrow adipocyte volume over total inner cavity volume in *Irx3*$^{-/-}$ and *Irx5*$^{-/-}$ mutants and corresponding controls. (*F–I*) Staining of Perilipin on distal tibia sections from P10 *Irx3*$^{-/-}$ and *Irx5*$^{-/-}$ mutants and corresponding controls. Scale bar = 100 μm. (*J*) Quantification of Perilipin$^+$ adipocytes in marrow space of *Irx3*$^{-/-}$ and *Irx5*$^{-/-}$ mutants and corresponding heterozygous littermate controls. Three nonconsecutive sections in each of five animals per genotype are quantified and the averaged data with standard deviations were presented in bar charts. Values of *p* calculated by Student's *t* test, two-tailed, unpaired. Scale bar = 100 μm.

composition of osteoblasts and adipocytes in bone marrow. Our data implicate the importance of these potent transcription factors in controlling cell-fate decisions during the lineage extension of chondrocytes, moderating the proportions of HC descendants favoring osteogenic lineage versus adipogenic fate. Upon depletion of *Irx3* and *Irx5*, HC-derived adipocytes are increased in the bone marrow, suggesting that IRX3 and IRX5, downstream of Wnt/β-catenin, act as molecular regulators of osteogenic lineage commitment of HC descendants via inhibiting adipogenic differentiation (Fig. 7*D*).

Bone marrow mesenchymal stem cells can give rise to osteoblasts and adipocytes. In humans, the rate of bone formation is negatively correlated with bone marrow adiposity and the adipocyte proportion is significantly increased in patients with osteoporosis.[57] Marrow adipogenesis initiates at the neonatal stage. Osteogenesis and adipogenesis compete with each other in mesenchymal cell fate commitment, and interrupting WNT signaling results in cell fate switching from osteoblasts to adipocytes.[52] Removal of β-catenin from early osteoblastic precursors results in arrested osteoblast differentiation,[19,21] while activation of Wnt signaling results in inhibition of preadipocyte differentiation into mature adipocytes via reducing PPARγ expression,[58] raising the possibility that Wnt signaling acts to control the cell fate of HCs toward osteoblastic and adipogenic progenitors. Recent studies have provided in vivo evidence that removal of β-catenin in the osteoblastic or chondrogenic lineages markedly reduced bone mass and increased bone marrow adipocytes.[23,52] Removal of β-catenin in HCs using a transgenic *Col10a1*-Cre mouse resulted in reduced bone and increased FABP4-expressing adipocytes associated with blood vessels.[23] However, the HC origin of adipocytes was not demonstrated.

The cell fate shift from osteoblasts to adipocytes found in the *Irx3/5* mutants led us to hypothesize that IRX3 and IRX5 act downstream of WNT signaling to determine the fate of chondrocytes in their lineage extension toward osteogenesis or adipogenesis (Fig. 7*D*). In *Irx3/5* mutants, osteoblast differentiation
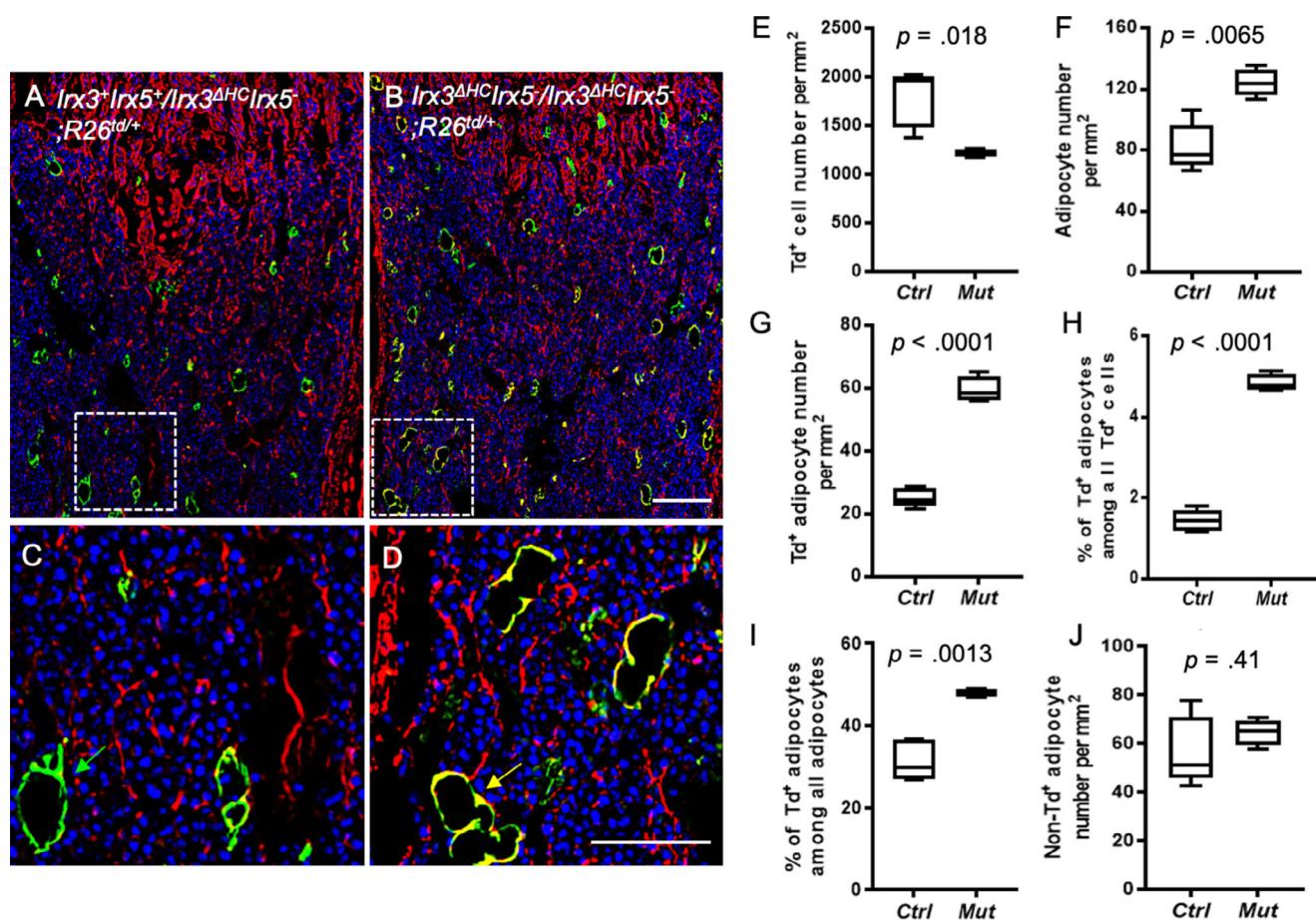
Fig 6. Depletion of *Irx3* and *Irx5* in HCs results in elevated amounts of bone marrow adipocytes derived from HCs. (A–D) Double staining of Perilipin (green) and tdTomato (td, red) on distal tibia sections from P10 *Irx3$^{\Delta HC}$Irx5$^-$/Irx3$^{\Delta HC}$Irx5$^-$;R26$^{td/+}$* mutants and control littermates. Perilipin$^+$ adipocytes from control (C) and mutant (D) mice are shown at higher magnification. The green and yellow arrows indicate non-HC-derived (Td$^-$/Perilipin$^+$) (C) and HC-derived (Td$^+$/Perilipin$^+$) (D) adipocytes, respectively. Scale bar = 100 μm. (E–J) Quantification of different populations in the bone marrow of P10 *Irx3$^{\Delta HC}$Irx5$^-$/Irx3$^{\Delta HC}$Irx5$^-$;R26$^{td/+}$* mutants and littermate controls. (E) Quantification of td$^+$ cells. (F) Quantification of total Perilipin$^+$ adipocytes. (G) Quantification of Perilipin$^+$/td$^+$ adipocytes. (H) Percentage of Perilipin$^+$/td$^+$ relative to total td$^+$ HC descendants. (I) Percentages of Perilipin$^+$/td$^+$ relative to total Perilipin$^+$ cells. (J) Quantification of Perilipin$^+$/td$^-$ adipocytes. Three nonconsecutive sections in each of five animals per genotype are quantified and the averaged data with standard deviations were presented in bar charts. Values of *p* calculated by Student's *t* test, two-tailed, unpaired.

was attenuated, with decreased HC-derived osteoblasts and increased HC-derived marrow adipocytes. The specific stage in the lineage extension process impacted by loss of *Irx3/5* is still unclear. Studies for the future would involve identification of the intermediate cell populations during the normal transition from HCs to osteoblasts, and determination of the associated gene regulatory networks, which would provide further insights into possible mechanisms by which these factors control HC to osteoblast transition and maintain the spectrum of skeletal stem/progenitor cells identified in developing and mature bones.[59–63] Identifying the molecular switches of osteogenesis and adipogenesis is particularly critical when formulating strategies to counteract aberrant lineage balance associated with pathological conditions such as osteoporosis, aging, and metabolic deficiency. It would be important to study if the effect on HC to osteoblast lineage decision persists with aging in mice as the progression of HCs to osteoblasts diminishes, and whether IRX3 and IRX5 also control cell fate decision during the bone

fracture healing when the HC to osteoblast transition also occurs.[8,10–12,64]

Bone marrow adipose tissue (MAT) has recently been regarded as another type of adipose tissue in addition to white adipose tissue (WAT) and brown adipose tissue (BAT), and serves as an endocrine organ regulating energy homeostasis, obesity, insulin resistance, inflammation, and immunity.[65–69] *Irx3* null mice show 30% loss of body fat mass and increased browning of WAT.[32] Intriguingly, we found increased numbers of bone marrow adipocytes in both *Irx3* and *Irx5* null mice, suggesting the correlation between MAT and body fat. Although the specific contribution of MAT to overall physiology and metabolic control is still unclear, it is thought to function as a special regulator of bone metabolism and may contribute to global metabolism.[66,68] Increased MAT is associated with lower bone mineral density and increased skeletal fragility in aging cohorts, and patients with osteoporosis or estrogen deficiency,[70] caloric restriction, anorexia nervosa,[71] or type 1 diabetes.[72] Patients
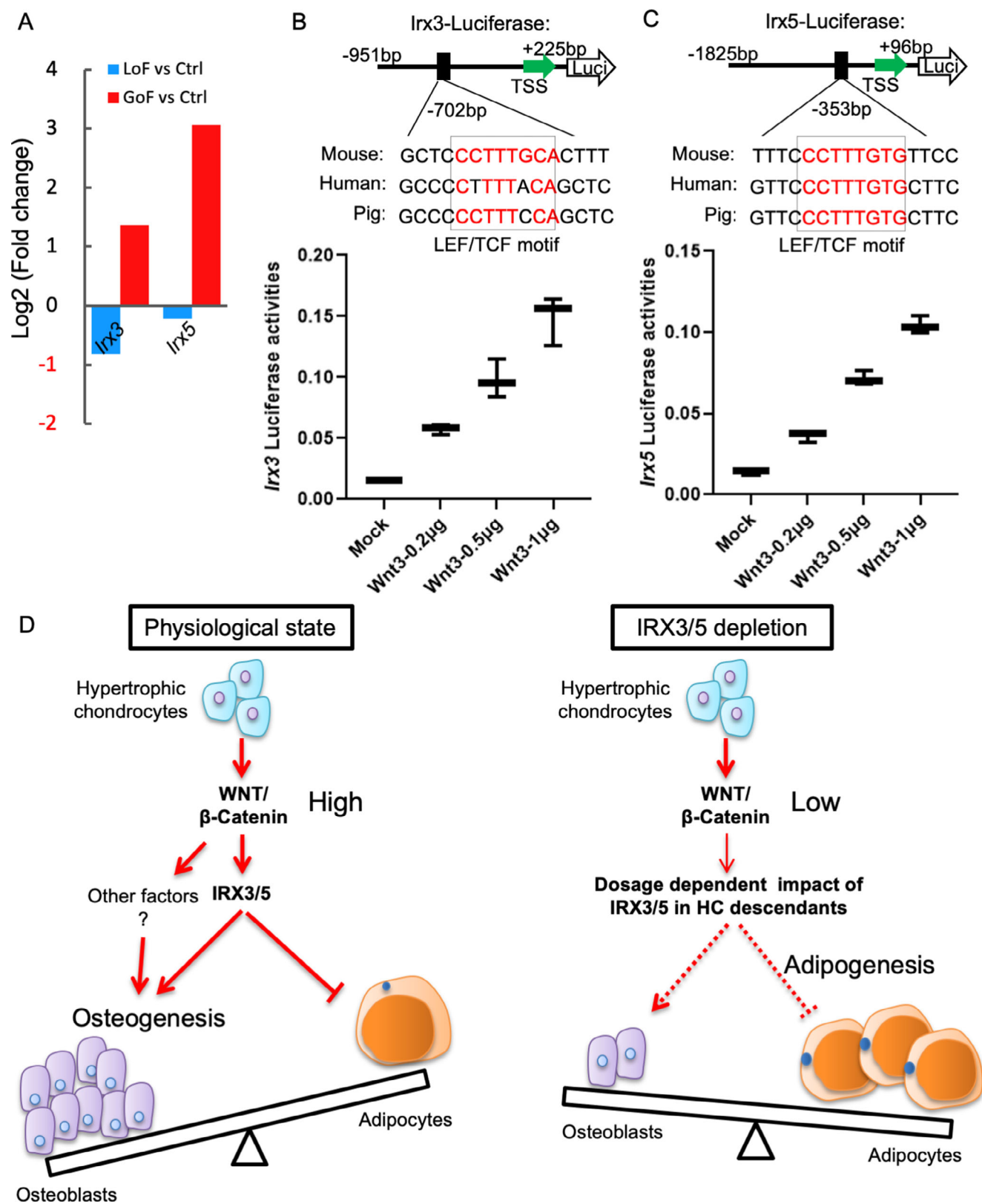
Fig 7. Transcriptional regulation of *Irx3* and *Irx5* by WNT/β-catenin. (*A*) Expression change of *Irx3* and *Irx5* in β-catenin loss of function and gain of function mutants compared to control by bulk RNA sequencing. (*B,C*) Luciferase assay on *Irx3* and *Irx5* promoters in ATDC5 cells showing concentration-dependent activation by recombinant Wnt3a. Equal amounts of expression plasmids were used for each well in three independent experiments. (*D*) Model of IRX3 and IRX5 in control of HC lineage progression and cell fate decision.

with IRX5 mutations showed skeletal anomalies with repeated long bone fractures.[28] Although the amount of MAT in these patients has not been assessed, our discovery of increased marrow adipocytes in *Irx3/5* mutant mice highlights the crucial role of *Irx3/5* in maintaining the balance between osteoblasts and adipocytes in bone. It is interesting that noncoding variation in the intronic region of the *FTO* gene can affect the adipocyte expression of *IRX3* and *IRX5*.[32,33,35,36] The association of the *FTO* variants with metabolic disease[32,33,35,36] raises the possibility that the impact may be associated with alterations in amounts of MAT regulated by IRX3/5.

The skewed proportion of HC-derived adipocytes compared to osteoblasts in the *Irx3/5* mutants suggests their roles in determining HC fate choice. It has been established that the HC to osteoblast transition also occurs in bone fracture repair in adult mice.[10] Mesenchymal stem cells are well known to be able to differentiate into adipocytes and osteoblasts. It is therefore possible that non–HC-derived mesenchymal stem cells in the bone marrow, when unable to express *Irx3/5*, may likewise adopt an adipogenic fate. Because increased marrow adiposity persists in older mice when the hypertrophic chondrocytes are largely reduced in number, a question arising is whether in humans, the impact of cell fate change when the growth plate is active may persist after growth plate closure and contribute to the development of disorders of low bone mass such as osteoporosis. The distinct functions of *Irx3* and *Irx5* in the control of body fat and MAT, and the connection between BAT, WAT and MAT, still require further investigation. Our study has extended implications for the specific roles of IRX3 and IRX5 in controlling balance of chondrocyte-derived osteoblasts and MAT. Future studies should exploit these findings to dissect the specific role of MAT and potential impact on whole-body metabolism by manipulating it independent of BAT and WAT. The identification of a β-catenin, IRX3 and IRX5 gene regulatory axis that controls the HC-osteoblast transition, ensuring osteogenesis over adipogenesis (Fig. 7*D*), has wide-ranging implications for bone biology and clinical application, with relevance to age-related bone loss, regeneration, and repair, bone diseases such as osteoporosis, and metabolic disorders such as obesity.

Disclosures

The authors state that they have no conflicts of interest.

Acknowledgments

Authors' roles: ZT, MK, SW, and KSEC conceived and designed the research studies. ZT, MK, and SW conducted the experiments and acquired the data. KYT generated RNAseq data and BN conducted bioinformatics analyses. ZT, MK, SW, KYT, and KSEC analyzed and interpreted the data. CCH provided *Irx 3/5* mice and reagents. ZT and KSEC wrote the original manuscript. MK, KT, DC, CCH, and CH helped with data interpretation and manuscript editing. KSEC acquired research funding and supervised the study.

Author Contributions: KSEC: Conceptualization; formal analysis; funding acquisition; project administration; resources; supervision; writing-original draft; writing-review and editing. ZT: Conceptualization; data curation; formal analysis; investigation; methodology; validation; writing-original draft; writing-review and editing. MK: Conceptualization; Data curation; formal analysis; investigation; methodology; validation; writing-original draft; writing-review and editing. SW: Conceptualization; Data curation; formal analysis; investigation; methodology; validation; writing-review and editing. KYT: Investigation; methodology; writing-review and editing. BN: Formal analysis; investigation; methodology; writing-review and editing. CH: Writing-review and editing. DC: Formal analysis; writing-review and editing. CCH: Formal analysis; resources; writing-review and editing.

Peer review

The peer review history for this article is available at https://publons.com/publon/10.1002/jbmr.4132.

References

1. Farnum CE, Wilsman NJ. Morphologic stages of the terminal hypertrophic chondrocyte of growth plate cartilage. Anat Rec. 1987;219 (3):221–32.

2. Ducy P, Amling M, Takeda S, et al. Leptin inhibits bone formation through a hypothalamic relay: a central control of bone mass. Cell. 2000;100(2):197–207.

3. Berger JM, Singh P, Khrimian L, et al. Mediation of the acute stress response by the skeleton. Cell Metab. 2019;30(5):890–902.e8.

4. Kronenberg HM. Developmental regulation of the growth plate. Nature. 2003;423:332–6.

5. Karsenty G, Kronenberg HM, Settembre C. Genetic control of bone formation. Annu Rev Cell Dev Biol. 2009;25:629–48.

6. Yip RKH, Chan D, Cheah KSE. Mechanistic insights into skeletal development gained from genetic disorders. Curr Top Dev Biol. 2019;133: 343–85.

7. Ono N, Ono W, Nagasawa T, Kronenberg HM. A subset of chondrogenic cells provides early mesenchymal progenitors in growing bones. Nat Cell Biol. 2014;16(12):1157–67.

8. Yang L, Tsang KY, Tang HC, Chan D, Cheah KS. Hypertrophic chondrocytes can become osteoblasts and osteocytes in endochondral bone formation. Proc Natl Acad Sci U S A. 2014;111(33):12097–102.

9. Mizuhashi K, Ono W, Matsushita Y, et al. Resting zone of the growth plate houses a unique class of skeletal stem cells. Nature. 2018;563 (7730):254–8.

10. Hu DP, Ferro F, Yang F, et al. Cartilage to bone transformation during fracture healing is coordinated by the invading vasculature and induction of the core pluripotency genes. Development. 2017;144 (2):221–34.

11. Hinton RJ, Jing Y, Jing J, Feng JQ. Roles of chondrocytes in endochondral bone formation and fracture repair. J Dent Res. 2017;96(1):23–30.

12. Zhou X, von der Mark K, Henry S, Norton W, Adams H, de Crombrugghe B. Chondrocytes transdifferentiate into osteoblasts in endochondral bone during development, postnatal growth and fracture healing in mice. PLoS Genet. 2014;10(12):e1004820.

13. Park J, Gebhardt M, Golovchenko S, et al. Dual pathways to endochondral osteoblasts: a novel chondrocyte-derived osteoprogenitor cell identified in hypertrophic cartilage. Biol Open. 2015;4(5):608–21.

14. Chan CKF, Gulati GS, Sinha R, et al. Identification of the human skeletal stem cell. Cell. 2018;175(1):43–56.e21.

15. Tsang KY, Chan D, Cheslett D, et al. Surviving endoplasmic reticulum stress is coupled to altered chondrocyte differentiation and function. PLoS Biol. 2007;5(3):e44.

IRX3 & IRX5 INHIBIT HYPERTROPHIC CHONDROCYTE ADIPOGENIC DIFFERENTIATION

16. Tsang KY, Cheah KS. The extended chondrocyte lineage: implications for skeletal homeostasis and disorders. Curr Opin Cell Biol. 2019;61:132–40.

17. Wolff LI, Hartmann C. A second career for chondrocytes-transformation into osteoblasts. Curr Osteoporos Rep. 2019;17(3):129–37.

18. Akiyama H, Kim JE, Nakashima K, et al. Osteo-chondroprogenitor cells are derived from Sox9 expressing precursors. Proc Natl Acad Sci U S A. 2005;102(41):14665–70.

19. Day TF, Guo X, Garrett-Beal L, Yang Y. Wnt/beta-catenin signaling in mesenchymal progenitors controls osteoblast and chondrocyte differentiation during vertebrate skeletogenesis. Dev Cell. 2005;8(5):739–50.

20. Zhou G, Zheng Q, Engin F, et al. Dominance of SOX9 function over RUNX2 during skeletogenesis. Proc Natl Acad Sci U S A. 2006;103(50):19004–9.

21. Hill TP, Spater D, Taketo MM, Birchmeier W, Hartmann C. Canonical Wnt/beta-catenin signaling prevents osteoblasts from differentiating into chondrocytes. Dev Cell. 2005;8(5):727–38.

22. Rodda SJ, McMahon AP. Distinct roles for Hedgehog and canonical Wnt signaling in specification, differentiation and maintenance of osteoblast progenitors. Development. 2006;133(16):3231–44.

23. Houben A, Kostanova-Poliakova D, Weissenbock M, et al. Beta-catenin activity in late hypertrophic chondrocytes locally orchestrates osteoblastogenesis and osteoclastogenesis. Development. 2016;143(20):3826–38.

24. Golovchenko S, Hattori T, Hartmann C, et al. Deletion of beta catenin in hypertrophic growth plate chondrocytes impairs trabecular bone formation. Bone. 2013;55(1):102–12.

25. Tan Z, Niu B, Tsang KY, et al. Synergistic co-regulation and competition by a SOX9-GLI-FOXA phasic transcriptional network coordinate chondrocyte differentiation transitions. PLoS Genet. 2018;14(4):e1007346.

26. Hamamy HA, Masri AT, Al-Hadidy AM, Ajlouni KM. Consanguinity and genetic disorders. Profile from Jordan. Saudi Med J. 2007;28(7):1015–7.

27. Hamamy HA, Teebi AS, Oudjhane K, Shegem NN, Ajlouni KM. Severe hypertelorism, midface prominence, prominent/simple ears, severe myopia, borderline intelligence, and bone fragility in two brothers: new syndrome. Am J Med Genet A. 2007;143A(3):229–34.

28. Bonnard C, Strobl AC, Shboul M, et al. Mutations in IRX5 impair craniofacial development and germ cell migration via SDF1. Nat Genet. 2012;44(6):709–13.

29. Gaborit N, Sakuma R, Wylie JN, et al. Cooperative and antagonistic roles for Irx3 and Irx5 in cardiac morphogenesis and postnatal physiology. Development. 2012;139(21):4007–19.

30. Li D, Sakuma R, Vakili NA, et al. Formation of proximal and anterior limb skeleton requires early function of Irx3 and Irx5 and is negatively regulated by Shh signaling. Dev Cell. 2014;29(2):233–40.

31. Cain CJ, Gaborit N, Lwin W, et al. Loss of Iroquois homeobox transcription factors 3 and 5 in osteoblasts disrupts cranial mineralization. Bone Rep. 2016;5:86–95.

32. Smemo S, Tena JJ, Kim KH, et al. Obesity-associated variants within FTO form long-range functional connections with IRX3. Nature. 2014;507(7492):371–5.

33. Claussnitzer M, Dankel SN, Kim KH, et al. FTO obesity variant circuitry and adipocyte browning in humans. N Engl J Med. 2015;373(10):895–907.

34. Bjune JI, Haugen C, Gudbrandsen O, et al. IRX5 regulates adipocyte amyloid precursor protein and mitochondrial respiration in obesity. Int J Obes (Lond). 2019;43(11):2151–62.

35. Dina C, Meyre D, Gallina S, et al. Variation in FTO contributes to childhood obesity and severe adult obesity. Nat Genet. 2007;39(6):724–6.

36. Frayling TM, Timpson NJ, Weedon MN, et al. A common variant in the FTO gene is associated with body mass index and predisposes to childhood and adult obesity. Science. 2007;316(5826):889–94.

37. Harada N, Tamai Y, Ishikawa T, et al. Intestinal polyposis in mice with a dominant stable mutation of the beta-catenin gene. EMBO J. 1999;18(21):5931–42.

38. Zhang SS, Kim KH, Rosen A, et al. Iroquois homeobox gene 3 establishes fast conduction in the cardiac His-Purkinje network. Proc Natl Acad Sci U S A. 2011;108(33):13576–81.

39. Madisen L, Zwingman TA, Sunkin SM, et al. A robust and high-throughput Cre reporting and characterization system for the whole mouse brain. Nat Neurosci. 2010;13(1):133–40.

40. Wai AW, Ng LJ, Watanabe H, Yamada Y, Tam PP, Cheah KS. Disrupted expression of matrix genes in the growth plate of the mouse cartilage matrix deficiency (cmd) mutant. Dev Genet. 1998;22(4):349–58.

41. Stickens D, Behonick DJ, Ortega N, et al. Altered endochondral bone development in matrix metalloproteinase 13-deficient mice. Development. 2004;131(23):5883–95.

42. Bagi CM, Hanson N, Andresen C, et al. The use of micro-CT to evaluate cortical bone geometry and strength in nude rats: correlation with mechanical testing, pQCT and DXA. Bone. 2006;38(1):136–44.

43. Scheller EL, Troiano N, Vanhoutan JN, et al. Use of osmium tetroxide staining with microcomputerized tomography to visualize and quantify bone marrow adipose tissue in vivo. Methods Enzymol. 2014;537:123–39.

44. Picelli S, Faridani OR, Bjorklund AK, Winberg G, Sagasser S, Sandberg R. Full-length RNA-seq from single cells using Smart-seq2. Nat Protoc. 2014;9(1):171–81.

45. Trapnell C, Roberts A, Goff L, et al. Differential gene and transcript expression analysis of RNA-seq experiments with TopHat and Cufflinks. Nat Protoc. 2012;7(3):562–78.

46. Anders S, Pyl PT, Huber W. HTSeq—a Python framework to work with high-throughput sequencing data. Bioinformatics. 2015;31(2):166–9.

47. Tanaka Y, Nakayamada S, Okada Y. Osteoblasts and osteoclasts in bone remodeling and inflammation. Curr Drug Targets Inflamm Allergy. 2005;4(3):325–8.

48. Giovannone D, Paul S, Schindler S, et al. Programmed conversion of hypertrophic chondrocytes into osteoblasts and marrow adipocytes within zebrafish bones. Elife. 2019;8:e42736.

49. Yang G, Zhu L, Hou N, et al. Osteogenic fate of hypertrophic chondrocytes. Cell Res. 2014;24(10):1266–9.

50. Scheller EL, Doucette CR, Learman BS, et al. Region-specific variation in the properties of skeletal adipocytes reveals regulated and constitutive marrow adipose tissues. Nat Commun. 2015;6:7808.

51. Cristancho AG, Lazar MA. Forming functional fat: a growing understanding of adipocyte differentiation. Nat Rev Mol Cell Biol. 2011;12(11):722–34.

52. Song L, Liu M, Ono N, Bringhurst FR, Kronenberg HM, Guo J. Loss of wnt/beta-catenin signaling causes cell fate shift of preosteoblasts from osteoblasts to adipocytes. J Bone Miner Res. 2012;27(11):2344–58.

53. Janssens S, Denayer T, Deroo T, Van Roy F, Vleminckx K. Direct control of Hoxd1 and Irx3 expression by Wnt/beta-catenin signaling during anteroposterior patterning of the neural axis in Xenopus. Int J Dev Biol. 2010;54(10):1435–42.

54. Nakamura Y, de Paiva Alves E, Veenstra GJ, Hoppler S. Tissue- and stage-specific Wnt target gene expression is controlled subsequent to beta-catenin recruitment to cis-regulatory modules. Development. 2016;143(11):1914–25.

55. Cadigan KM, Waterman ML. TCF/LEFs and Wnt signaling in the nucleus. Cold Spring Harb Perspect Biol. 2012;4(11):a007906.

56. Shukunami C, Ishizeki K, Atsumi T, Ohta Y, Suzuki F, Y H. Cellular hypertrophy and calcification of embryonal carcinoma-derived chondrogenic cell line ATDC5 in vitro. J Bone Miner Res. 1997;12(8):1174–88.

57. Justesen J, Stenderup K, Ebbesen EN, Mosekilde L, Steiniche T, Kassem M. Adipocyte tissue volume in bone marrow is increased with aging and in patients with osteoporosis. Biogerontology. 2001;2(3):165–71.

58. Ross SE, Hemati N, Longo KA, et al. Inhibition of adipogenesis by Wnt signaling. Science. 2000;289(5481):950–3.

59. Chan CK, Chen CC, Luppen CA, et al. Endochondral ossification is required for haematopoietic stem-cell niche formation. Nature. 2009;457(7228):490–4.

60. Zhou BO, Yue R, Murphy MM, Peyer JG, Morrison SJ. Leptin-receptor-expressing mesenchymal stromal cells represent the main source of

bone formed by adult bone marrow. Cell Stem Cell. 2014;15(2): 154–68.

61. Marecic O, Tevlin R, McArdle A, et al. Identification and characterization of an injury-induced skeletal progenitor. Proc Natl Acad Sci U S A. 2015;112(32):9920–5.

62. Worthley DL, Churchill M, Compton JT, et al. Gremlin 1 identifies a skeletal stem cell with bone, cartilage, and reticular stromal potential. Cell. 2015;160(1–2):269–84.

63. Shi Y, He G, Lee WC, McKenzie JA, Silva MJ, Long F. Gli1 identifies osteogenic progenitors for bone formation and fracture repair. Nat Commun. 2017;8(1):2043.

64. Aghajanian P, Mohan S. The art of building bone: emerging role of chondrocyte-to-osteoblast transdifferentiation in endochondral ossification. Bone Res. 2018;6:19.

65. Bukowska J, Frazier T, Smith S, et al. Bone marrow adipocyte developmental origin and biology. Curr Osteoporos Rep. 2018;16(3):312–9.

66. Li Y, Meng Y, Yu X. The unique metabolic characteristics of bone marrow adipose tissue. Front Endocrinol. 2019;10:69.

67. Tilg H, Moschen AR. Adipocytokines: mediators linking adipose tissue, inflammation and immunity. Nat Rev Immunol. 2006;6(10):772–83.

68. Sulston RJ, Cawthorn WP. Bone marrow adipose tissue as an endocrine organ: close to the bone? Horm Mol Biol Clin Investig. 2016;28 (1):21–38.

69. Cawthorn WP, Scheller EL, Parlee SD, et al. Expansion of bone marrow adipose tissue during caloric restriction is associated with increased circulating glucocorticoids and not with Hypoleptinemia. Endocrinology. 2016;157(2):508–21.

70. Schwartz AV. Marrow fat and bone: review of clinical findings. Front Endocrinol. 2015;6:40.

71. Ghali O, Al Rassy N, Hardouin P, Chauveau C. Increased bone marrow adiposity in a context of energy deficit: the tip of the iceberg? Front Endocrinol. 2016;7:125.

72. Cawthorn WP, Scheller EL, Learman BS, et al. Bone marrow adipose tissue is an endocrine organ that contributes to increased circulating adiponectin during caloric restriction. Cell Metab. 2014; 20(2):368–75.